

Research Articles: Cellular/Molecular

Indirect effects of Halorhodopsin activation: potassium redistribution, non-specific inhibition and spreading depolarisation

<https://doi.org/10.1523/JNEUROSCI.1141-22.2022>

Cite as: J. Neurosci 2022; 10.1523/JNEUROSCI.1141-22.2022

Received: 10 June 2022

Revised: 28 November 2022

Accepted: 2 December 2022

This Early Release article has been peer-reviewed and accepted, but has not been through the composition and copyediting processes. The final version may differ slightly in style or formatting and will contain links to any extended data.

Alerts: Sign up at www.jneurosci.org/alerts to receive customized email alerts when the fully formatted version of this article is published.

1 Indirect effects of Halorhodopsin activation: potassium
 2 redistribution, non-specific inhibition and spreading depolarisation

3 R. Ryley Parrish^{1,2}, Connie Mackenzie-Gray-Scott¹, Tom Jackson-Taylor¹, Alex Grundmann¹, Faye
 4 McLeod¹, Neela K. Codadu⁴, Alexandru Călin¹, Hannah Alfonsa¹, Rob C. Wykes^{3,4}, Juha Voipio⁵,
 5 Andrew J. Trevelyan¹ *

6
 7 1. Newcastle University Biosciences Institute, Medical School, Framlington Place, Newcastle
 8 upon Tyne, NE2 4HH, UK.

9 2. Department of Cell Biology and Physiology, Brigham Young University, Provo, Utah

10 3. Nanomedicine Lab, University of Manchester, Manchester M13 9PL, UK

11 4. Queen Square Institute of Neurology, University College London, WC1N 3BG, UK

12 5. Faculty of Biological and Environmental Sciences, Molecular and Integrative Biosciences,
 13 University of Helsinki, 00014 Helsinki, Finland

14
 15 **Orcid Numbers:**

16 Parrish	0000-0001-6798-6140
17 Mackenzie-Gray-Scott	0000-0001-7962-8906
18 McLeod	0000-0003-0379-7476
19 Codadu	0000-0002-5819-0340
20 Calin	0000-0003-2363-2898
21 Alfonsa	0000-0002-6357-7494
22 Wykes	0000-0002-6141-6822
23 Voipio	0000-0001-7096-1286
24 Trevelyan	0000-0001-9307-4241

25
 26 * Correspondence to andrew.trevelyan@ncl.ac.uk

27 Abbreviated title: Indirect effects of Halorhodopsin activation

28 Number of pages

29 Number of figures: 7

30 Number of tables

31 Number of words

Indirect effects of Halorhodopsin activation

32 Abstract 248 words

33 Introduction 626 words

34 Discussion 908 words

35 The authors declare no conflicts of interest

36 **Acknowledgments:** The work was supported by grants from BBSRC (BB/P019854/1), MRC
37 (MR/R005427/1), and the European Union's Horizon 2020 research and innovation program
38 (Grant Agreement No. 881603, GrapheneCore3). AC was supported by an NIHR funding -
39 Academic Clinical Fellowship in Neurology.

40 We would like to thank the support staff in the animal facilities at both Newcastle University
41 and UCL. We also thank Dr Anton Guimera-Brunet and Dr Eduard Masvidal-Codina (Institut de
42 Microelectronica de Barcelona, CNM-CSIC) for providing the graphene micro-transistor arrays
43 used in this study, and Dr Martin Smith (UCL) for technical assistance in preparing the mice for
44 the graphene micro-transistor array *in vivo* experiments. We thank Joe Raimondo for
45 commenting on drafts of this manuscript and discussion.

46 **Abstract**

47 The movement of ions in and out of neurons can exert significant effects on neighboring
48 cells. Here we report several experimentally important consequences of activation of the
49 optogenetic chloride pump, Halorhodopsin. We recorded extracellular K^+ concentration,
50 $[K^+]_{\text{extra}}$, in neocortical brain slices prepared from young adult mice (both sexes) which express
51 Halorhodopsin in pyramidal cells. Strong Halorhodopsin activation induced a pronounced
52 drop in $[K^+]_{\text{extra}}$, that persisted for the duration of illumination. Pharmacological blockade of
53 K^+ channels reduced the amplitude of this drop, indicating that it represents K^+ redistribution
54 into cells during the period of hyperpolarization. Halorhodopsin thus drives the inward
55 movement of both Cl^- directly, and K^+ secondarily. When the illumination period ended, a
56 rebound surge in extracellular $[K^+]$ developed over tens of seconds, partly reflecting the
57 previous inward redistribution of K^+ , but additionally driven by clearance of Cl^- coupled to K^+
58 by the potassium-chloride co-transporter, KCC2. The drop in $[K^+]_{\text{extra}}$ during light activation
59 leads to a small (2-3mV) hyperpolarization also of other cells that do not express
60 Halorhodopsin. Its activation therefore has both direct and indirect inhibitory effects.
61 Finally, we show that persistent strong activation of Halorhodopsin causes cortical spreading
62 depolarisations (CSDs), both *in vitro* and *in vivo*. This novel means of triggering CSDs is
63 unusual, in that the events can arise during the actual period of illumination, when neurons
64 are being hyperpolarized and $[K^+]_{\text{extra}}$ is low. We suggest that this fundamentally different
65 experimental model of CSDs will open up new avenues of research to explain how they occur
66 naturally.

67 **Significance statement**

68 Halorhodopsin is a light-activated electrogenic chloride pump, which has been widely
69 used to inhibit neurons optogenetically. Here, we demonstrate three previously unrecognized
70 consequences of its use: 1. Intense activation leads to secondary movement of K^+ ions into the
71 cells. 2. The resultant drop in extracellular $[K^+]$ reduces excitability also in other, non-expressing
72 cells. 3. Intense persistent Halorhodopsin activation can trigger cortical spreading

Indirect effects of Halorhodopsin activation

73 depolarization (CSD). Halorhodopsin-induced CSDs can occur when neurons are hyperpolarized
74 and extracellular $[K^+]$ is low. This contrasts with the most widely used experimental models that
75 trigger CSDs with high $[K^+]$. Both models, however, are consistent with the hypothesis that CSDs
76 arise following net inward ionic movement into the principal neuron population.

77 **Introduction**

78 The complexity of neuronal behaviour derives in large measure from the fact that
79 neurons do not act in isolation. This is most apparent in the form of synaptic interactions, but
80 in certain circumstances, the neurons may also exert significant effects on neighbouring cells
81 through indirect means, arising from movement of ions in or out of the extracellular space
82 (Jefferys, 1995). Neuronal firing and synaptic activity leads to large ionic movement across the
83 neuronal membrane (Attwell and Laughlin, 2001; Hodgkin and Huxley, 1952), and if sufficiently
84 intense, can result in significant redistribution of key ions, with depletion of extracellular Na^+
85 and Ca^{2+} ions, and rises in extracellular K^+ ions.

86 The development of optogenetics has provided a new set of research tools for
87 investigating such matters, with novel ways to challenge neuronal networks (Deisseroth, 2011).
88 Optogenetic studies have mostly involved network level analyses, in which specific
89 subpopulations of neurons are either activated or inactivated to dissect out their roles in large
90 networks or whole animals. Cellular processes can also be examined using optogenetics, and in
91 this regard, the light activated ion pumps (Chow et al., 2010; Zhang et al., 2007) offer
92 particularly interesting ways to challenge the cells experimentally, either in isolation or in
93 tandem with ion channels. The light activated chloride pump, Halorhodopsin can be used to
94 drive chloride into neurons (Alfonsa et al., 2015; Raimondo et al., 2012), whereas chloride
95 extrusion can be achieved by coupling the action of the light activated proton pump and the
96 opening of a chloride channel, using a co-operative opsin called Cl-out (Alfonsa et al., 2016).
97 We reasoned that artificial chloride manipulation provides a further means of examining the
98 relationship between chloride entry and delayed extracellular $[K^+]$ rises via the potassium
99 chloride cotransporter (KCC2), that have to date only been examined by means of GABAergic
100 activation (Chang et al., 2018; Shiri et al., 2015; Viitanen et al., 2010). Specifically, we

Indirect effects of Halorhodopsin activation

101 hypothesized that Halorhodopsin-mediated ion redistribution would lead to increased KCl
102 efflux by KCC2, revealing itself as a surge in extracellular K^+ concentration, $[K^+]_{\text{extra}}$, after
103 illumination ends. To test this hypothesis, we utilized mice in which Halorhodopsin was
104 expressed in all pyramidal cells, under the Emx1 promoter (Gorski et al., 2002), and recorded
105 changes in $[K^+]_{\text{extra}}$ using ion-sensitive electrodes (Voipio et al., 1994).

106 These studies confirmed the relationship between intracellular $[Cl^-]$ and extracellular $[K^+]$
107 transients, but further revealed three other, previously unrecognized, consequences of
108 activation of optogenetic pumps. The first is that intense activation of Halorhodopsin leads to
109 redistribution of K^+ ions into neurons through K^+ ion channels, on account of the
110 hyperpolarization of a large population of neurons altering the balance between inward and
111 outward fluxes of ions; this is particularly evident for K^+ on account of it being highly permeant
112 at resting E_m , and its low basal extracellular concentration. An important consequence of the K^+
113 redistribution is that the lowering of $[K^+]_{\text{extra}}$ causes a hyperpolarisation of all neurons, not just
114 those that express the opsin; this represents a form of indirect inhibition by Halorhodopsin.
115 Finally, we report that Halorhodopsin activation can also trigger cortical spreading
116 depolarisation (CSD) events. Our initial observations of Halorhodopsin-triggered CSDs were of
117 events arising immediately after the end of illumination, but of particular note were other
118 instances, when CSDs arose even during the Halorhodopsin activation, when most neurons in
119 the network were strongly hyperpolarized and $[K^+]_{\text{extra}}$ was low. As such, this novel way of
120 triggering CSDs, by a hyperpolarizing photocurrent, is quite unlike most other known natural
121 and experimental triggers (e.g. ischaemia trauma, seizures (Somjen, 2004; Ullah et al., 2015))
122 where the common thread has been considered to be raised $[K^+]_{\text{extra}}$ and strong depolarization
123 (Tamim et al., 2021). The exception is the triggering of CSDs by application of hypotonic
124 solution, leading to the suggestion that osmotic stress may be the critical factor (Chebabo et al.,
125 1995; Somjen, 2004), a hypothesis that is consistent with the data we present here.

126 **Methods**

127 **Ethical Approval:** All procedures performed were in accordance with the guidelines of the
128 Home Office UK and Animals (Scientific Procedures) Act 1986 and approved by the Animal

Indirect effects of Halorhodopsin activation

129 Welfare and Ethical Review Body at both Newcastle University and UCL. Male and female mice
130 were used for experimentation.

131 **Slice Preparation:** We used both wild-type C57BL/6 mice, and also mice expressing eNpHR3.0
132 within the pyramidal cell population, generated by cross-breeding homozygous Emx1-cre mice
133 (Jackson Laboratory, Stock 005628) with mice containing a floxed STOP cassette in front of an
134 eNpHR3.0/EYFP domain (Jackson Laboratory, Stock 014539; both maintained on the C57BL/6
135 background). Emx1-promoter yields gene expression only in pyramidal cells in neocortex, in
136 adult mice, although it can drive gene expression in glia in other brain areas, and early in
137 development (Gorski et al., 2002). Experiments were performed on mice aged 1 - 8 months, of
138 both sexes. Mice were sacrificed by Schedule 1 method, brains were removed and placed in
139 cold cutting solution containing (in mM): 3 MgCl₂; 126 NaCl; 2.6 NaHCO₃; 3.5 KCl; 1.26
140 NaH₂PO₄; 10 glucose. 400 μm horizontal sections were made on a Leica VT1200 vibratome
141 (Leica Microsystem, Germany). Slices were stored at room temperature, in an interface holding
142 chamber for 1 – 4 hours prior to experimentation. Solutions were bubbled with carbogen (95%
143 O₂ and 5% CO₂) in artificial cerebro-spinal fluid (aCSF) containing (in mM): 2 CaCl₂; 1 MgCl₂; 126
144 NaCl; 26 NaHCO₃; 3.5 KCl; 1.26 NaH₂PO₄; 10 glucose.

145 **In vitro Extracellular recordings:** Extracellular recordings were performed using an interface
146 recording chamber. Slices were placed in the recording chamber and perfused with aCSF
147 supplemented in different experiments with various combinations of the following drugs: 1μM
148 Tetrodotoxin (TTX) (Abcam), 10μM VU 0463271 (Tocris Bioscience), 10mM
149 tetraethylammonium (TEA) (Sigma), 2mM Ba²⁺ (Fisons plc, England), as indicated in the results
150 section. Recordings were obtained using aCSF-filled ~1-3MΩ borosilicate glass microelectrodes
151 (GC120TF-10; Harvard apparatus, Kent) placed in deep layers of neocortex. Extracellular
152 potassium, [K⁺]_{extra}, was measured using single-barrelled K⁺-selective microelectrodes. The
153 pipettes were pulled from nonfilamented borosilicate glass (Harvard Apparatus, Kent, UK), and
154 the glass was exposed to vapor of dimethyl-trimethyl-silylamine (Sigma-Aldrich), baking at 200^o
155 C for 40 minutes. The pipettes were then backfilled with aCSF. A short column of the K⁺ sensor
156 (Potassium ionophore I, cocktail B; Sigma-Aldrich, #99373) was taken into the tip of the
157 salinized pipette by using slight suction. The recordings through the K⁺-sensor electrode were

Indirect effects of Halorhodopsin activation

158 referenced to a second electrode filled with aCSF. From the differential signal from a custom
159 build amplifier, we calculated the $[K^+]_{\text{extra}}$ from calibration recordings made in an open bath,
160 using sudden increments in $[K^+]_{\text{extra}}$. This provided a scaling factor S , of 55-59mV, where the K^+
161 concentration at a given moment in time, t , was calculated from the differential voltage, $V(t)$, as
162 follows:

$$163 [K] = [K]_{\text{baseline}} 10^{V(t)/S}$$

164 $[K]_{\text{baseline}}$ for our experiments was 3.5 mM. The temperature of the chamber and perfusate was
165 maintained at 33-36°C using a closed circulating heater (FH16D, Grant instruments, Cambridge,
166 UK). The solutions were perfused at the rate of 3 ml/min by a Watson Marlow 501U peristaltic
167 pump (Watson-Marlow Pumps Limited, Cornwall UK). The direct current local field potential
168 signal was unfiltered and amplified to a 10X output with a custom build amplifier. These
169 waveform signals were digitized with a Micro 1401-3 ADC board (Cambridge Electronic Design,
170 UK) and Spike2 version 7.10 software (Cambridge Electronic Design, UK). Signals were sampled
171 at 10 kHz. Recordings were analysed using a custom-written code in MATLAB (Mathworks, MA,
172 USA).

173 ***In vitro* patch clamp recordings:** Brain slices were prepared, from the same mice strain (Halo^{Fl} x
174 Emx1-Cre), as follows. Mice were anaesthetised by intraperitoneal injection of ketamine (75
175 mg kg⁻¹, Ketalar™ Injection, Pfizer Ltd., Sandwich, UK) combined with medetomidine (1 mg kg⁻¹,
176 Domitor®, Janssen Animal Health, Basingstoke, UK), and perfused through the heart using a
177 chilled and aerated “sucrose aCSF” (in mM: 228 sucrose; 26 NaHCO₃; 4 MgCl₂; 3 KCl; 1.25
178 NaH₂PO₄; 10 glucose) for 1 minute, before removing the brain, and making 350µm coronal
179 brain slices in the same sucrose solution. Slices were then incubated in a submerged chamber
180 in conventional 1mM Mg²⁺ / 2mM Ca²⁺ aCSF, at room temperature. For the recordings, slices
181 were transferred to a recording chamber held on a movable top plate (Scientifica) with
182 mounted electrode micromanipulators (Scientifica). Slices were visualized, and illuminated,
183 through a UMPanFL N 40x, 0.5 NA objective (Olympus, UK), using a Scientifica upright
184 microscope fitted with a spinning disk confocal attachment (Visitech, UK) and a Hamamatsu
185 C9100 EM camera (Hamamatsu Photonics, Japan) and coordinated using Visitech software. The
186 temperature in the recording chamber was maintained at 32-34°C by warming the perfusate

Indirect effects of Halorhodopsin activation

187 (delivered at 3-5mls/min) using a heated sleeve immediately prior to the recording chamber,
188 and with the additional aid of a plate heater (Warner Instruments). Whole cell recordings of
189 neurons from the temporal association area were made using 4-7M Ω pipettes. Pipettes were
190 filled with a KMeSO₄-based internal solution containing (mM): 125 KMeSO₄, 6 NaCl, 10 HEPES,
191 2.5 Mg-ATP, 0.3 Na₂-GTP. Osmolarity and pH of all the internal solutions used were adjusted to
192 284mOsm and 7.4. The offset of the patch clamp amplifier was zeroed prior to patching the
193 cells, and we adjusted the subsequent measurement of membrane potential, therefore, by the
194 liquid junction potential, which was calculated using LJPCalc software
195 (<https://swharden.com/LJPCalc>) to be 9.6mV, according to the stationary Nernst-Planck
196 equation (Marino et al., 2014). The eNPHR3.0 was conjugated to an eYFP fluorescent marker,
197 allowing us to discriminate between cells that expressed the opsin (pyramidal cells), and those
198 that did not (presumptive interneurons and some glia). After going whole cell, we recorded in
199 current clamp mode, first testing the optogenetic response to a short (200ms) illumination with
200 568nm light, and then the firing response to a current injected through the patch electrode.
201 We then assessed the response to a more intense, and sustained illumination with both 488nm
202 and 568nm wavelength light together. We used this combination because previous work
203 indicated that concurrent illumination with both yellow and blue light yields a more sustained
204 eNPHR3.0 photocurrent, because the blue light refreshes the opsin (Han and Boyden, 2007). In
205 non-expressing, fast-spiking interneurons, we finally tested the firing response to 200pA
206 current either in darkness, or under steady-state illumination with 488nm and 568nm light.
207 Patch clamp data was collected using a Multiclamp 700B amplifier (Axon Instruments,
208 Molecular Probes), digitized using a 1401 AD converter and recorded onto a Dell Precision
209 Desktop computer. Recordings were analysed offline, using custom-written codes in
210 Matlab2018b. The input-output functions were fitted with sigmoidal equation, as follows:

$$F = \frac{F_{max}}{(1 + e^{(\sigma - I)/N})}$$

211 Where F is the firing rate, I is the current, and the fitting procedure used a non-linear least
212 squares process to derive the other three parameters: maximal firing rate (F_{max}), the current

Indirect effects of Halorhodopsin activation

213 giving half-maximal firing (σ) and a parameter which dictates the slope (N ; note, high values
214 give shallower slopes).

215 ***In vivo* Extracellular recordings:** Animals were anaesthetised with urethane (20% w/v in saline
216 for injection at 0.1ml/gram of mouse) and placed on a stereotaxic frame with heating pad,
217 monitored with a rectal probe to maintain body temperature. A cranial window was created on
218 the left hemisphere and an LFP electrode was placed into the somatosensory cortex. DC LFP
219 recordings were performed as in the *in vitro* experiments, with the electrode about 1mm deep
220 into the tissue. No mice were used past 4 hours from urethane injection.

221 **Optogenetic illumination for extracellular recordings:** Optogenetic illumination was performed
222 using a Fiber-coupled LED light at 565 nm (Thorlabs, M565F3) and driven by an LED driver
223 (Thorlabs, LEDD1) placed in trigger mode. Light output was measured at an average of 9 mW.
224 The LED light was position just above the superficial layers of the neocortex for the slice
225 experiments and pointed toward the deep layers, where the extracellular recordings were
226 performed. For the *in vivo* experiments, the LED was placed in the somatosensory cortex, just
227 above the tissue and about 2mm from the recording electrode. Optogenetic activation was
228 from 90 seconds to 5 minutes depending on the experiment.

229 ***In vivo* recordings in awake head-fixed mice using graphene micro-transistor arrays:**

230 C57BL/6 mice (~3-4 months of age), were injected with 500nl of rAAV5-hSyn-eNpHR3.0-eYFP
231 (UNC vector core) unilaterally into the primary motor cortex (M1) and headbars attached.
232 Three weeks later, we initiated rounds of habituation to the Neurotar fixation frame (Neurotar,
233 Finland). Once the animal was fully habituated, a second surgery was performed to allow a
234 craniotomy over the ipsilateral somatosensory and visual cortex. Upon recovery from this
235 surgery (3-4hrs), the animal was placed in the neurotar frame, a 16-channel graphene micro-
236 transistor array positioned over the craniotomy (dura intact), and a fiber optic cannula,
237 connected to a Thorlabs green (594nm) LED positioned over a small bur hole made over the M1
238 area. Optogenetic or pinprick induction of CSD was induced in the motor cortex and
239 electrographically recorded using the graphene transistor arrays over ipsilateral somatosensory
240 and visual cortex - see (Masvidal-Codina et al., 2021) for full surgical, experimental and
241 graphene transistor data analysis details).

Indirect effects of Halorhodopsin activation

242 **Statistics:** Statistical analysis of electrophysiology was performed using GraphPad Prism
243 (GraphPad Software, Inc., La Jolla, CA, USA). Data was analysed with a Mann-Whitney test, a
244 Kruskal-Wallis with a Dunn's multiple comparisons test, or a paired t-test where appropriate.
245 Figures of electrophysiology traces were created in Matlab2015b or 2018b (Mathworks, MA,
246 USA). Statistics are expressed as the mean \pm standard error of mean (s.e.m.).

247 **Results**248 **Activation of Halorhodopsin causes secondary redistribution of K^+ ions**

249 Previous work showed that intense GABAergic activation is followed by a surge in $[K^+]_{\text{extra}}$
250 (Chang et al., 2018; Shiri et al., 2015; Viitanen et al., 2010). The explanation for this is that Cl^-
251 ions which moved into neurons through the GABA receptors are then extruded coupled to K^+
252 via KCC2. This hypothesized mechanism predicts that a similar surge in $[K^+]_{\text{extra}}$ should occur if
253 neurons are artificially loaded with Cl^- using the optogenetic chloride pump, Halorhodopsin
254 (Alfonsa et al., 2015; Raimondo et al., 2012). We prepared brain slices from adult mice which
255 expressed Halorhodopsin in all pyramidal cells, under the Emx1 promoter, and measured
256 $[K^+]_{\text{extra}}$ during and after a 90s illumination epoch (Figure 1). In all slices, we recorded large
257 increases in $[K^+]_{\text{extra}}$, peaking at a mean 8.0 ± 0.44 mM (mean \pm s.e.m.; $n = 14$ slices). The surge
258 was relatively slow, peaking only 59.9 ± 10.4 s after the end of the period of illumination. We
259 also observed a drop in $[K^+]_{\text{extra}}$, that persisted throughout the entire period of illumination.
260 Brain slices from wild-type mice showed no change in $[K^+]_{\text{extra}}$ during periods of equivalent
261 illumination ($n = 3$ slices; Figure 1A).

262 We first investigated the nature of the drop in $[K^+]_{\text{extra}}$ during the period of illumination.
263 We performed these experiments in the presence of TTX, to rule out any possible contribution
264 arising from altered levels of neuronal firing during activation of Halorhodopsin. In the
265 presence of TTX alone, the $[K^+]_{\text{extra}}$ dropped to 1.71 ± 0.08 mM ($\Delta K_{\text{extra}} = \sim -1.8$ mM from the
266 baseline level of 3.5mM), compared to 2.8 ± 0.09 mM in TEA ($\Delta K_{\text{extra}} = \sim -0.7$ mM), and $2.85 \pm$
267 0.11 mM when Ba^{2+} was added ($\Delta K_{\text{extra}} = \sim -0.65$ mM; Figure 2). Glial K^+ channels are relatively
268 insensitive to TEA, so the fact that the addition of Ba^{2+} ions was not significantly different from

Indirect effects of Halorhodopsin activation

269 the effect of TEA alone suggests that most of the drop in $[K^+]_{\text{extra}}$ occurs via a hyperpolarization-
270 driven redistribution of K^+ into neurons. This is consistent with the pattern of opsin expression
271 in these animals, driven under the Emx1 promoter, which in adults, appears limited to the
272 pyramidal population (Gorski et al., 2002). Whole cell patch clamp recordings of
273 Halorhodopsin-expressing pyramidal neurons recorded light-induced hyperpolarization by
274 24.5 ± 1.5 mV (mean \pm sem; range 10 - 34 mV, 23 cells, from 6 mice) from resting membrane
275 potential (-62.1 ± 1.5 mV; during intense illumination $E_m = -84.9 \pm 2.5$ mV (range = -64 to -
276 104mV; Figure 3A)).

277 Non-specific inhibitory effects of Halorhodopsin activation

278 We further reasoned that the drop in the extracellular $[K^+]$ may have indirect effects also
279 upon non-expressing cells, because the reduced $[K^+]_{\text{extra}}$ would be expected to lower their E_m .
280 To examine this possibility, we prepared brain slices in which Halorhodopsin was expressed in
281 the pyramidal population, but made targeted patch-clamp recordings of non-expressing cells
282 (Figure 3): non-pyramidal neurons (interneurons (n = 15), indicated by firing patterns and the
283 lack of a prominent Halorhodopsin response, and also glia (n = 2), indicated by non-firing
284 response to current injection. We found that during these periods of illumination, there was
285 also a small, but significant hyperpolarization of non-expressing cells of 2.0 ± 0.3 mV (n = 17
286 cells, comprising 2 glia (hyperpolarized by 2.0 and 3.6mV respectively) and 15 interneurons (E_m
287 = -62.4 ± 1.0 mV), from 6 mice; range of hyperpolarizing effect = 0 to 3.6mV) which was both
288 significantly different from the null response ($p = 6.9 \times 10^{-6}$, Student's t-test), and also
289 significantly smaller than the pyramidal response ($p = 7.2 \times 10^{-14}$; Student's t-test). No change
290 was seen during illumination in wild-type brain slices, which lack Halorhodopsin. A possible
291 explanation for the small hyperpolarising effect in the non-pyramidal population is that there
292 was a low level of "breakthrough" expression of Halorhodopsin in these cells. If that were the
293 explanation, though, the kinetics of the change in E_m would be comparable to that seen in
294 pyramidal cells, since this is dictated primarily at the molecular level, rather than the level of
295 expression. Notably, the time-course of the hyperpolarization of "non-expressing" cells was
296 very slow, reaching its peak level at 1061 ± 150 ms (n = 13 interneurons - discounting the two

Indirect effects of Halorhodopsin activation

297 cells which showed no discernible shift in E_m ; the two glia reached peak effect at 800 and
298 870ms respectively) after the start of illumination, in marked contrast to a rapid peak
299 hyperpolarization achieved in pyramidal cells, which occurred at just 47.6 ± 5.6 ms ($n = 23$)
300 which was highly significantly faster than in non-expressing cells ($p = 3.2 \times 10^{-10}$, Student's t-
301 test). The slow evolving hyperpolarizing effect in the non-expressing cells had a similar time
302 course to the drop in $[K^+]_{\text{extra}}$, and so we concluded that this was indeed due to indirect effects,
303 and not due to break-through expression in cells without the Emx1 promoter.

304 We reasoned that the drop in $[K^+]_{\text{extra}}$ may also influence neuronal firing in non-expressing
305 neurons. To test this, we measured the input-output function, in fast-spiking interneurons
306 (FSIs), in response to step changes in somatically injected current, in baseline conditions and
307 during a sustained period of pyramidal-Halorhodopsin activation ($n = 9$ cells, 6 mice; Figure 4).
308 Consistently, we found that firing rates was reduced, in these non-expressing cells, when the
309 tissue was illuminated, consistent with our results regarding the drop in $[K^+]_{\text{extra}}$ (Figure 2) and
310 also of E_m in non-expressing cells (Figure 3). This was the case if the effect was quantified either
311 by the total number of spikes in the 1s current injection (Figure 4Bi) or as the maximal
312 instantaneous firing rate (reciprocal of the shortest interspike interval) (Figure 4Bii). For each
313 cell, we fitted a sigmoidal function (Figure 4Ci) to the input-output functions for both conditions
314 (light vs no light; see Methods for fitting details). In every case, the half-maximal current was
315 increased during periods of illumination to activate Halorhodopsin in the pyramidal population
316 (Figure 4Cii,iii; 9/9 cells; mean increase = 12.7 ± 3.3 %; significantly different from null
317 response, $p = 0.0049$). Across the 9 cells, there was no significant change in either the maximal
318 firing rate ($p = 0.20$), or the slope of the fit ($p = 0.37$), in the two conditions (light vs no light).

319 A large rebound surge in $[K^+]_{\text{extra}}$ follows Halorhodopsin activation

320 We next examined the nature of the large rebound surge in peak $[K^+]_{\text{extra}}$, following
321 Halorhodopsin activation (range 2.0 – 7.1 mM above baseline, 3.5 mM). One component of the
322 rebound surge will be extrusion of K^+ ions that moved into the neurons during the period of
323 illumination. Notably, however, in a set of experiments with 90s illumination, when the
324 illumination-induced lowering of $[K^+]_{\text{extra}}$ reaches a steady state, there was no correlation

Indirect effects of Halorhodopsin activation

325 between the amplitude of the illumination-induced drop in $[K^+]_{\text{extra}}$, and the rebound surge in
326 $[K^+]_{\text{extra}}$ ($R^2 = 0.006$, $p = 0.79$).

327 A second explanation is that the rebound $[K^+]_{\text{extra}}$ surge was caused by rebound spiking
328 following a period of hyperpolarization. However, the large post-Halorhodopsin surge persisted
329 in the presence of the Na^+ channel blocker, tetrodotoxin (TTX), indicating that rebound spiking
330 was not the source of the rebound peak in $[K^+]_{\text{extra}}$. In contrast, the peak was substantially
331 reduced, although not abolished, by blocking the K^+ - Cl^- co-transporter, KCC2, using VU0463271
332 ($p=0.0037$, Kruskal-Wallis test with a Dunn's multiple comparisons test). The post-illumination
333 peak in $[K^+]_{\text{extra}}$ was also reduced by the K^+ channel blocker, TEA (Figures 4C,D; $p = 0.0064$,
334 Kruskal-Wallis test with a Dunn's multiple comparisons test). The time to the peak of the
335 rebound in $[K^+]_{\text{extra}}$ was delayed by blocking KCC2 (Figure 4C, $p = 0.0014$, two-tailed paired t-
336 test) , but not by blocking K^+ channels (Figure 4D, $p = 0.61$, two-tailed paired t-test).
337 Altogether, our data showing a large surge in $[K^+]_{\text{extra}}$, following a period of Halorhodopsin
338 chloride-loading, are entirely consistent with the previous report of a secondary rise in
339 $[K^+]_{\text{extra}}$, following chloride-loading occurring naturally caused by intense GABAergic activation
340 (Viitanen et al., 2010).

341

342

343 Induction of spreading depolarization events by Halorhodopsin activation

344 While performing these investigations of Halorhodopsin-induced K^+ redistribution, we
345 observed that cortical spreading depolarization (CSD) events often occurred shortly after
346 periods of illumination (Figure 6A). This happened relatively unusually with shorter illumination
347 epochs (10-30s), but when the period of illumination were extended to 90s, CSDs occurred in
348 around 33% of trials. Notably, we were able to induce CSDs also in the presence of TTX alone (n
349 = 5 brain slices, from 4 mice), with TTX, TEA and Ba^{2+} together (to additionally block K^+
350 channels, $n = 3$ brain slices, from 2 mice), with TTX and KCC2 blocked using VU 0463271 (1 brain
351 slice), and with blockade of both glutamatergic and GABAergic neurotransmission in the
352 presence of TTX (1 brain slice).

Indirect effects of Halorhodopsin activation

353 Using synchronous measurements of the LFP and also the $[K^+]_{\text{extra}}$, we estimated that at
354 the moment the CSD started, the median $[K^+]_{\text{extra}}$ locally was 3.1 mM (interquartile range = 2.5 –
355 3.5 mM; full range = 2.1 – 17 mM; 19 brain slices, from 8 mice; Figure 6B), and occurred shortly
356 after (1.73 ± 1.91 s latency) the end of a period of illumination (typically <100s illumination).
357 Remarkably, if the illumination was maintained, then CSDs occurred in every slice ($n = 6$ slices,
358 from 2 mice) with a latency of 526 ± 79.6 s. In contrast, CSDs were not induced by 600s
359 illumination with 565nm light either in brain slices from wild-type mice ($n = 6$ slices, from 1
360 mouse), or from mice expressing channelrhodopsin-eYFP ($n = 12$ slices, from 2 mice). In each
361 case, light was delivered at a spot, and notably, post hoc staining for DAPI, NeuN and GFAP
362 revealed no inhomogeneity of stain at that site, either in Halorhodopsin slices that experienced
363 CSDs ($n = 12$ slices, from 2 animals) or from the wild-type and channelrhodopsin-eYFP mice.
364 The significance of CSDs occurring during periods of Halorhodopsin activation, is that at this
365 time, the expressing population of pyramidal neurons is hyperpolarized by the direct action of
366 the opsin, and the $[K^+]_{\text{extra}}$ is below baseline.

367 Notably, spreading depolarisations could be induced using this same method, *in vivo*, in
368 anaesthetized adult mice expressing Halorhodopsin in pyramidal neurons. Illumination was
369 directed onto the cortical surface, having performed a craniotomy, and with the dura removed
370 to allow penetration of the electrode. In these experiments, the light fibre was out of the brain,
371 fractionally above its surface. The period of illumination required to induce CSDs varied from
372 animal to animal, but once we had established the requisite duration in an individual animal,
373 this same stimulation consistently triggered CSDs thereafter, having allowed at least 15 mins
374 recovery between events ($n = 4$ mice).

375 In a final set of *in vivo* experiments, we recorded CSD propagation in awake head-fixed
376 mice ($n = 3$) using multichannel graphene micro-transistor arrays (Masvidal-Codina et al., 2021),
377 thereby avoiding any confounders that may arise from anesthesia. We recorded events using a
378 4x4 graphene microarray placed upon the cortical surface. Data were collected at 16 bits,
379 allowing a wide dynamic range in DC recordings (without saturating the signal), while retaining
380 adequate voltage resolution. As such, these devices allow wide-bandwidth detection of
381 electrographic signals and are suitable for recording spreading depolarisations and higher

Indirect effects of Halorhodopsin activation

382 frequency activity concurrently (Figure 6Ci,ii respectively). We examined how Halo-induced
383 CSDs compared to those triggered by physical trauma, in this case, by a brief pin-prick to the
384 cortical surface. In these recordings, CSDs induced by the two different methods appeared
385 virtually identical at the individual transistors (Figure 6Ciii). We concluded therefore that even
386 though the method of induction differed, once established, the actual events were equivalent.

387 **Discussion**

388 The direct effect of illumination of Halorhodopsin is well established: that it drives an
389 inward movement of chloride ions, causing the cell to become hyperpolarized. This has been
390 used in many previous studies to inhibit neuronal activity. Here we show that there are also
391 indirect effects, but that these may have useful experimental value for probing neuronal
392 pathophysiological mechanisms. The first of these is that sustained Halorhodopsin activation
393 causes a lowering of extracellular K^+ levels. In all such cases, a steady state occurs when inward
394 ionic movement equals the outward movement. In normal baseline conditions, there is a
395 continuous small drift of K^+ ions out of the cell through leak channels, driven by the difference
396 between the membrane potential, E_m , and E_K . Since this is a steady state, it must be balanced
397 by continual inward movement of K^+ ions by other means, the most important of which is the
398 Na^+-K^+ ATPase (Larsen et al., 2014). During the illumination, hyperpolarization alters the leak
399 current driving force ($E_K - E_m$), reducing the outward movement of K^+ initially, and even
400 reversing its direction (to an inward movement) once E_m drops below E_K . The time course of
401 the K^+ redistribution is likely to have a complex relationship to the action of the Halorhodopsin
402 pump, since it is affected both by its hyperpolarizing, and also its chloride-loading, actions; the
403 latter effect will increase K^+ extrusion via KCC2, even during the period of illumination, and so
404 counter the K^+ entry previously mentioned. There may further be redistribution of K^+ through
405 the glial network that could affect how quickly the system reaches a steady state.

406 A consequence of this drop in $[K^+]_{extra}$ is a measurable reduction in excitability of non-
407 expressing neurons in the local vicinity. This consequence is important to recognize, when
408 interpreting the inhibitory consequences of Halorhodopsin, because not all the effects may be
409 attributable to the specific subpopulation of neurons expressing the opsin. Having said that, it

Indirect effects of Halorhodopsin activation

410 is also pertinent that our experiments used tissue with Halorhodopsin expressed in the
411 pyramidal population, which constitutes about 80% of the neuronal population, in murine
412 neocortex. The effect is likely to be far weaker with sparse expression patterns, and also will
413 critically depend upon the intensity of illumination.

414 We further show that following cessation of Halorhodopsin stimulation, there was a very
415 marked rebound rise in $[K^+]_{\text{extra}}$. This likely constitutes, in part, a return to the extracellular
416 space of some of the K^+ that had entered the cell. The size of the overshoot beyond resting
417 $[K^+]_{\text{extra}}$ indicates that this is further boosted by cells extruding K^+ coupled to Cl^- extrusion,
418 mediated by KCC2, as has shown in several previous publications following intense GABAergic
419 activation (Viitanen et al., 2010). The rebound $[K^+]_{\text{extra}}$ may also contribute to the excess
420 network excitability following Halorhodopsin, that has previously been noted (Alfonso et al.,
421 2015; Raimondo et al., 2012).

422 An interesting, and unanticipated finding was the final effect, which is that protracted,
423 intense activation of Halorhodopsin proves to be a very reliable means of triggering CSDs, both
424 *in vitro* and *in vivo*. The significance of this new way of triggering CSDs is that it differs
425 fundamentally from what has been a prevailing hypotheses of CSD initiation: the critical point is
426 that instances of CSDs arising during the actual period of illumination demonstrate that they
427 can develop from a point where all the pyramidal cells are hyperpolarized and the $[K^+]_{\text{extra}}$ is
428 actually below baseline levels (i.e. $< 3.5\text{mM}$). CSDs are thought to underlie spreading migraine
429 auras (Lauritzen et al., 2011), and have also been described following both ischaemic and
430 haemorrhagic strokes (Dreier, 2011; Lemale et al., 2022), and seizures (Dreier and Reiffurth,
431 2015; Hablitz and Heinemann, 1989; Mody et al., 1987; Tamim et al., 2021). They were first
432 described by Leao (Leao, 1944, 1947), with the early realization that they could be triggered by
433 increasing $[K^+]_{\text{extra}}$, leading to the idea that a strong depolarization was the means of induction
434 and propagation. Latterly, a more nuanced view is evolving (Dreier and Reiffurth, 2015; Lemale
435 et al., 2022; Somjen, 2004), taking into account other ways in which CSDs may be triggered,
436 such as raised osmotic tension within neurons. Our main findings are consistent with this
437 hypothesis, by describing a process whereby a continuous electrogenic pump, driving first Cl^- ,
438 and secondarily K^+ ions into neurons, triggers the CSD, but fall short of a conclusive proof of the

Indirect effects of Halorhodopsin activation

439 theory. New experimental models, however, often provide the impetus for new insights, and
440 we suggest that Halorhodopsin induction could fuel research into how CSDs arise naturally. One
441 important instance is where CSDs arise from seizure activity. Persistently intense neuronal
442 activity, as occurs during seizures, results in a large net movement of ions into cells, the
443 opening of pannexin channels in neuronal membranes (Thompson et al., 2008), allowing
444 movement of large molecules such as fluorescent dyes, and likely also allowing water to follow.
445 This, in turn, leads to cell swelling and a substantial drop in the extracellular space (Andrew and
446 MacVicar, 1994; Iwasa et al., 1980; Somjen, 2004). Indeed, the change in the tissue impedance
447 due to this redistribution can be used to characterize the spatial-temporal extent of
448 pathological discharges (Witkowska-Wrobel et al., 2021). An important research question
449 remains regarding the relationship of CSDs with seizure activity (Dreier and Reiffurth, 2015).
450 Superficially, seizure activity and Halorhodopsin activation appear rather different in terms of
451 the effects on membrane potential, but share an important feature that in both, there is a net
452 influx of ions into neurons.

453 **Figures and Table**

454 **Figure 1. Activation of Halorhodopsin in principal cell class induces strong modulation of**
 455 **extracellular $[K^+]_e$, during and after illumination.**

456 (A) Recordings of extracellular $[K^+]_e$ in brain slices in which either Halorhodopsin (blue, top), was
 457 expressed in all pyramidal cells, or in a slice with no opsin expression (black, bottom). Yellow
 458 bar represents the time of illumination (90s period). Light activation of Halorhodopsin induced
 459 a very marked reduction in $[K^+]_e$, followed by an even larger, rebound increase. . Brain slices
 460 without opsins showed no light induced fluctuations in $[K^+]_e$. (B) The peak extracellular $[K^+]_e$,
 461 after the end of the period of Halorhodopsin activation (mean peak = 7.98mM).

462 **Figure 2. The main movement of K^+ ions from the extracellular space, induced by opsin**
 463 **activation is through K^+ channels.**

464 (A) Recordings of extracellular $[K^+]_e$ during a period of Halorhodopsin activation in the presence
 465 of TTX and additionally TEA and Ba^{2+} , to block different K^+ channels. Note the far smaller
 466 change in extracellular $[K^+]_e$ when K channels were blocked. (B) Measurements of the minimum
 467 level of extracellular $[K^+]_e$ in the different pharmacological conditions ($p = 0.0021$ for TTX vs TTX
 468 + TEA and $p = 0.0015$ for TTX vs TTX / TEA vs TTX / TEA / Ba^{2+} , Kruskal-Wallis test with a Dunn's
 469 multiple comparisons test).

470

471 **Figure 3. The light-induced drop in extracellular $[K^+]_e$ indirectly affects the membrane potential**
 472 **and excitability of cells that do not express Halorhodopsin.**

473 (A) Whole cell current clamp recordings of a pyramidal cell (black), a fast-spiking interneuron
 474 (red) and a glial cell, made from neocortical brain slices prepared from mice which express
 475 Halorhodopsin in all pyramidal cells, but not in other cell classes. In each case, intense light
 476 activation was delivered diffusely to an area of several hundred microns around the cell
 477 location, through the microscope objective. Panel Ai illustrates the very large amplitude
 478 hyperpolarisation in the pyramidal cells (the baseline E_m for the three recordings are
 479 superimposed, for ease of comparison of the light induced effect; pyramidal $E_m = -63$ mV;
 480 interneuronal $E_m = -70.5$ mV; glial $E_m = -68.5$ mV), and the far smaller effect on the non-

Indirect effects of Halorhodopsin activation

481 expressing cell classes, while Aii shows the same plots normalised to the maximal drop, in order
 482 to illustrate the difference in time course of the effects on E_m . (B) Bar charts showing the
 483 difference in the amplitude (Bi, $p = 7.2 \times 10^{-14}$; Student's t-test) and the time to peak (Bii, $p = 3.2$
 484 $\times 10^{-10}$; Student's t-test) of the hyperpolarisation in the Halo-expressing pyramidal cells ($n = 23$),
 485 and the non-expressing interneurons ($n = 15$).
 486

487 **Figure 4. Indirect suppression of firing in non-expressing, fast spiking interneurons.**

488 (A) Firing response to current injection (200pA, 1s) in a fast-spiking interneuron that did not
 489 express Halorhodopsin, in control conditions (black) or while there was concurrent activation of
 490 Halorhodopsin in the local pyramidal cells. (B) Input-output (IO) functions of a different fast-
 491 spiking interneuron, plotted as the total number of action potentials during the 1s period of
 492 current injection (Bi), or as the maximal instantaneous firing rate (reciprocal of the shortest
 493 interspike interval) (Bii). In both cases, the IO function was derived without illumination (black)
 494 and then with concurrent activation of Halorhodopsin in the pyramidal population (red, "light").
 495 (Ci) The IO function (see methods). (Cii) Paired (light / no light) values of the half-maximal
 496 current (I_{50}) for each cell, and the same data, normalised to the no-light I_{50} ($p < 10^{-6}$, paired t-
 497 test).
 498

499 **Figure 5. Halorhodopsin-induced K^+ redistribution involves KCC2 and voltage-activated K^+**
 500 **channels.**

501 (A) Recordings of $[K^+]_{extra}$ during and after a 90s period of Halorhodopsin activation (yellow bar)
 502 in the presence of the Na^+ channel blocker, TTX (blue, top), or the KCC2 blocker, VU0463271
 503 (red, middle), or the blocker of voltage-gated K^+ channels, TEA (black, bottom). (B) The peak
 504 $[K^+]_{extra}$, after the end of illumination, for the three different drugs ($p = 0.0037$ for TTX vs TTX +
 505 VU and $p = 0.0064$ for TTX vs TTX + TEA, Kruskal-Wallis test with a Dunn's multiple comparisons
 506 test).
 507 (C) The time to the peak $[K^+]_{extra}$, following a 90s period of Halorhodopsin activation, with and
 508 without the presence of the KCC2 blocker, VU0463271. Blockade of KCC2 causes a significant
 509 delay in the time to the peak ($p = 0.0014$, Two-tailed paired t-test). All experiments were
 510 performed in the presence of the Na^+ channel blocker, TTX, to exclude any contribution to the

Indirect effects of Halorhodopsin activation

511 [K⁺] fluxes made by rebound neuronal spiking. (D) Similar measurements made with and
512 without the voltage-gated K⁺ channel blocker, TEA, showing no significant effect.
513

514 **Figure 6. Prolonged activation of Halorhodopsin in pyramidal populations can trigger cortical**
515 **spreading depolarisations.**

516 (A) Concurrent recordings of extracellular K^+ concentration (Ai), and the local field potential
517 (Aii), during a 90s activation of Halorhodopsin in the pyramidal population, in which a CSD
518 event developed soon after the illumination period ended. (B) The $[K^+]_{\text{extra}}$ at the start of the
519 CSD for the different drug groupings (Bi), and its time of initiation (Bii) relative to the end of a
520 90s long period of Halorhodopsin activation (each data point is a single brain slice). (C) Example
521 traces of a CSD triggered *in vivo*, recorded using a graphene multi-transistor array, which
522 started while illumination was still on-going (illumination was started ~250s prior to the start of
523 the event). The top panel shows both low (Ci) and high (Cii) frequency components, to
524 illustrate how these different bandwidths can help distinguish between depolarization (the
525 voltage deflection in Ci) and depression (the reduced high frequency component in Cii). (Ciii)
526 Illustration of the propagation across multiple electrodes. The dotted line is aligned to the
527 maximal deflection of the leading electrode, to help visualize the relative delays of onset in the
528 other electrodes. A second CSD was triggered locally by a pin-prick injury, and recorded through
529 the same array. The right panel shows the overlaid electrophysiological signatures of the two
530 events, recorded through the different transistors, to illustrate the similar time course for the
531 Halo- and pinprick induced events, at each individual site (note that for the right panels, we
532 aligned the recordings to their start; Scale bars, 50s, 50 μ V).

533 **References**

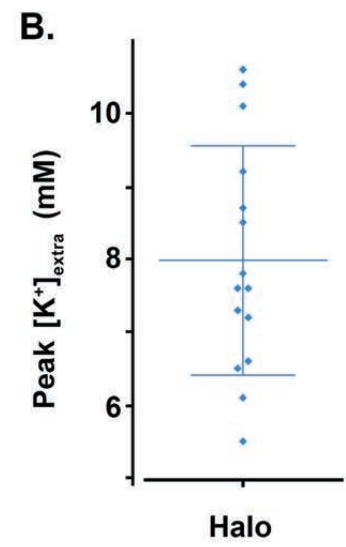
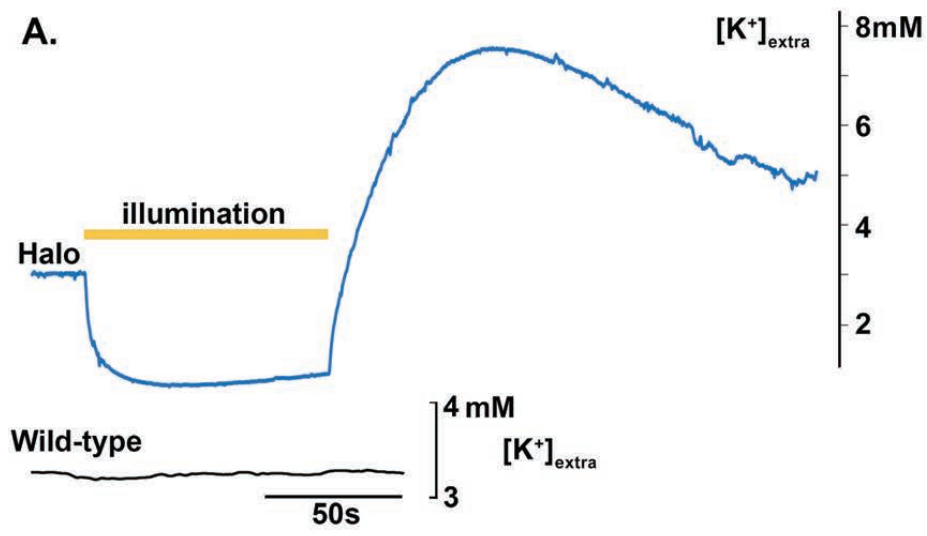
- 534 Alfonsa, H., Lakey, J.H., Lightowers, R.N., and Trevelyan, A.J. (2016). Cl-out is a novel
535 cooperative optogenetic tool for extruding chloride from neurons. *Nature communications* 7,
536 13495.
- 537 Alfonsa, H., Merricks, E.M., Codadu, N.K., Cunningham, M.O., Deisseroth, K., Racca, C., and
538 Trevelyan, A.J. (2015). The contribution of raised intraneuronal chloride to epileptic network
539 activity. *J Neurosci* 35, 7715-7726.
- 540 Andrew, R.D., and MacVicar, B.A. (1994). Imaging cell volume changes and neuronal excitation
541 in the hippocampal slice. *Neuroscience* 62, 371-383.
- 542 Attwell, D., and Laughlin, S.B. (2001). An energy budget for signaling in the grey matter of the
543 brain. *J Cereb Blood Flow Metab* 21, 1133-1145.
- 544 Chang, M., Dian, J.A., Dufour, S., Wang, L., Moradi Chameh, H., Ramani, M., Zhang, L., Carlen,
545 P.L., Womelsdorf, T., and Valiante, T.A. (2018). Brief activation of GABAergic interneurons
546 initiates the transition to ictal events through post-inhibitory rebound excitation. *Neurobiol Dis*
547 109, 102-116.
- 548 Chebabo, S.R., Hester, M.A., Aitken, P.G., and Somjen, G.G. (1995). Hypotonic exposure
549 enhances synaptic transmission and triggers spreading depression in rat hippocampal tissue
550 slices. *Brain Res* 695, 203-216.
- 551 Chow, B.Y., Han, X., Dobry, A.S., Qian, X., Chuong, A.S., Li, M., Henninger, M.A., Belfort, G.M.,
552 Lin, Y., Monahan, P.E., *et al.* (2010). High-performance genetically targetable optical neural
553 silencing by light-driven proton pumps. *Nature* 463, 98-102.
- 554 Deisseroth, K. (2011). Optogenetics. *Nat Methods* 8, 26-29.
- 555 Dreier, J.P. (2011). The role of spreading depression, spreading depolarization and spreading
556 ischemia in neurological disease. *Nat Med* 17, 439-447.
- 557 Dreier, J.P., and Reiffurth, C. (2015). The stroke-migraine depolarization continuum. *Neuron* 86,
558 902-922.
- 559 Gorski, J.A., Talley, T., Qiu, M., Puellas, L., Rubenstein, J.L., and Jones, K.R. (2002). Cortical
560 excitatory neurons and glia, but not GABAergic neurons, are produced in the Emx1-expressing
561 lineage. *J Neurosci* 22, 6309-6314.
- 562 Hablitz, J.J., and Heinemann, U. (1989). Alterations in the microenvironment during spreading
563 depression associated with epileptiform activity in the immature neocortex. *Brain Res Dev Brain*
564 *Res* 46, 243-252.
- 565 Han, X., and Boyden, E.S. (2007). Multiple-color optical activation, silencing, and
566 desynchronization of neural activity, with single-spike temporal resolution. *PLoS One* 2, e299.
- 567 Hodgkin, A.L., and Huxley, A.F. (1952). Currents carried by sodium and potassium ions through
568 the membrane of the giant axon of Loligo. *J Physiol* 116, 449-472.
- 569 Iwasa, K., Tasaki, I., and Gibbons, R.C. (1980). Swelling of nerve fibers associated with action
570 potentials. *Science* 210, 338-339.
- 571 Jefferys, J.G. (1995). Nonsynaptic modulation of neuronal activity in the brain: electric currents
572 and extracellular ions. *Physiol Rev* 75, 689-723.

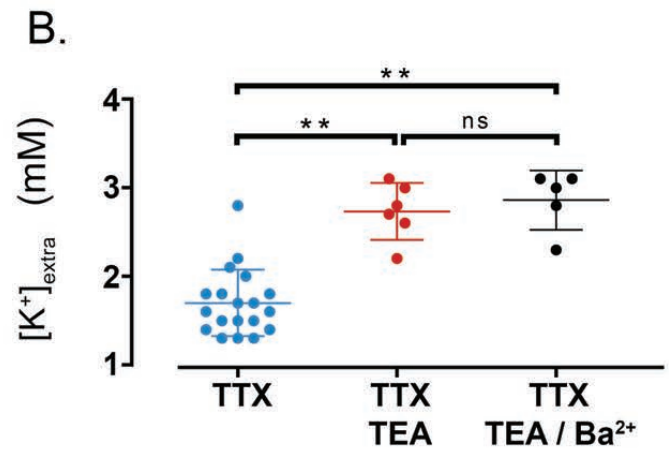
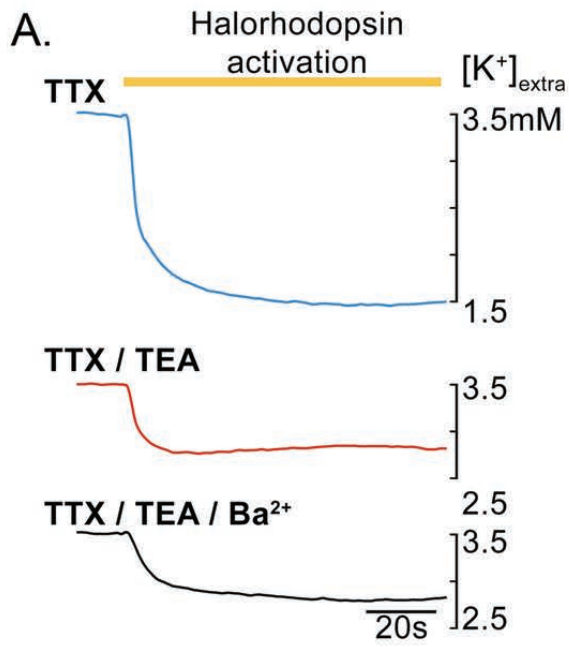
Indirect effects of Halorhodopsin activation

- 573 Larsen, B.R., Assentoft, M., Cotrina, M.L., Hua, S.Z., Nedergaard, M., Kaila, K., Voipio, J., and
574 MacAulay, N. (2014). Contributions of the Na(+)/K(+)-ATPase, NKCC1, and Kir4.1 to
575 hippocampal K(+) clearance and volume responses. *Glia* 62, 608-622.
- 576 Lauritzen, M., Dreier, J.P., Fabricius, M., Hartings, J.A., Graf, R., and Strong, A.J. (2011). Clinical
577 relevance of cortical spreading depression in neurological disorders: migraine, malignant
578 stroke, subarachnoid and intracranial hemorrhage, and traumatic brain injury. *J Cereb Blood*
579 *Flow Metab* 31, 17-35.
- 580 Leao, A.A. (1944). Spreading depression of activity in the cerebral cortex. *J Neurophysiol* 7, 359-
581 390.
- 582 Leao, A.A. (1947). Further observations on the spreading depression of activity in the cerebral
583 cortex. *J Neurophysiol* 10, 409-414.
- 584 Lemale, C.L., Luckl, J., Horst, V., Reiffurth, C., Major, S., Hecht, N., Woitzik, J., and Dreier, J.P.
585 (2022). Migraine Aura, Transient Ischemic Attacks, Stroke, and Dying of the Brain Share the
586 Same Key Pathophysiological Process in Neurons Driven by Gibbs-Donnan Forces, Namely
587 Spreading Depolarization. *Frontiers in cellular neuroscience* 16, 837650.
- 588 Marino, M., Misuri, M., and Brogioli, D. (2014). A new open source software for the calculation
589 of the liquid junction potential between two solutions according to the stationary Nernst-Planck
590 equation. arXiv:14033640v2.
- 591 Masvidal-Codina, E., Smith, T.M., Rathore, D., Gao, Y., Illa, X., Prats-Alfonso, E., Corro, E.D.,
592 Calia, A.B., Rius, G., Martin-Fernandez, I., *et al.* (2021). Characterization of optogenetically-
593 induced cortical spreading depression in awake mice using graphene micro-transistor arrays.
594 *Journal of neural engineering* 18.
- 595 Mody, I., Lambert, J.D., and Heinemann, U. (1987). Low extracellular magnesium induces
596 epileptiform activity and spreading depression in rat hippocampal slices. *J Neurophysiol* 57,
597 869-888.
- 598 Raimondo, J.V., Kay, L., Ellender, T.J., and Akerman, C.J. (2012). Optogenetic silencing strategies
599 differ in their effects on inhibitory synaptic transmission. *Nat Neurosci* 15, 1102-1104.
- 600 Shiri, Z., Manseau, F., Levesque, M., Williams, S., and Avoli, M. (2015). Interneuron activity leads
601 to initiation of low-voltage fast-onset seizures. *Ann Neurol* 77, 541-546.
- 602 Somjen, G.G. (2004). *Ions in the brain: Normal function, seizures and stroke* (Oxford: Oxford
603 University Press).
- 604 Tamim, I., Chung, D.Y., de Moraes, A.L., Loonen, I.C.M., Qin, T., Misra, A., Schlunk, F., Endres, M.,
605 Schiff, S.J., and Ayata, C. (2021). Spreading depression as an innate antiseizure mechanism.
606 *Nature communications* 12, 2206.
- 607 Thompson, R.J., Jackson, M.F., Olah, M.E., Rungta, R.L., Hines, D.J., Beazely, M.A., MacDonald,
608 J.F., and MacVicar, B.A. (2008). Activation of pannexin-1 hemichannels augments aberrant
609 bursting in the hippocampus. *Science* 322, 1555-1559.
- 610 Ullah, G., Wei, Y., Dahlem, M.A., Wechselberger, M., and Schiff, S.J. (2015). The Role of Cell
611 Volume in the Dynamics of Seizure, Spreading Depression, and Anoxic Depolarization. *PLoS*
612 *Comput Biol* 11, e1004414.
- 613 Viitanen, T., Ruusuvaori, E., Kaila, K., and Voipio, J. (2010). The K+-Cl cotransporter KCC2
614 promotes GABAergic excitation in the mature rat hippocampus. *J Physiol* 588, 1527-1540.

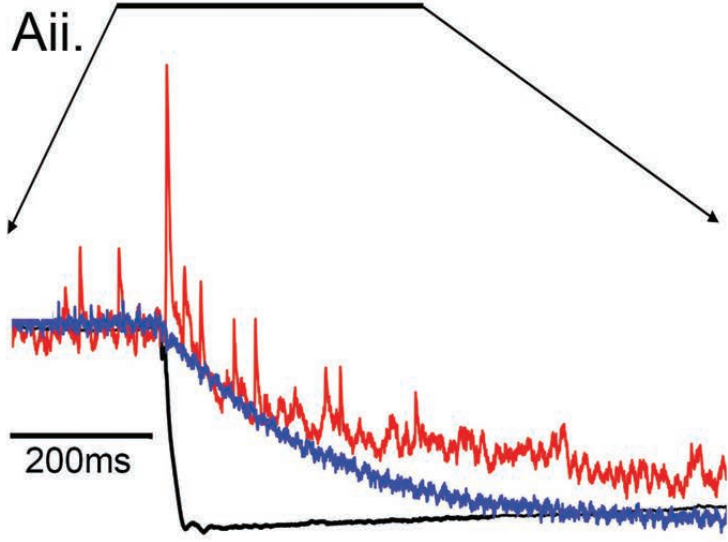
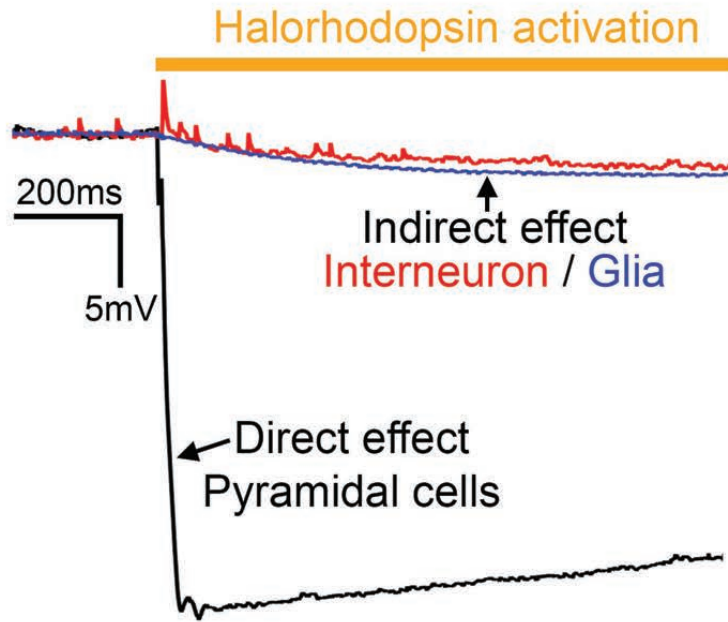
Indirect effects of Halorhodopsin activation

- 615 Voipio, J., Pasternack, M., and MacLeod, K. (1994). Ion-sensitive microelectrodes. In
616 Microelectrode Techniques, The Plymouth Workshop Handbook, D. Ogden, ed. (The Company
617 of Biologists).
- 618 Witkowska-Wrobel, A., Aristovich, K., Crawford, A., Perkins, J.D., and Holder, D. (2021). Imaging
619 of focal seizures with Electrical Impedance Tomography and depth electrodes in real time.
620 *Neuroimage* 234, 117972.
- 621 Zhang, F., Wang, L.P., Brauner, M., Liewald, J.F., Kay, K., Watzke, N., Wood, P.G., Bamberg, E.,
622 Nagel, G., Gottschalk, A., *et al.* (2007). Multimodal fast optical interrogation of neural circuitry.
623 *Nature* 446, 633-639.
624

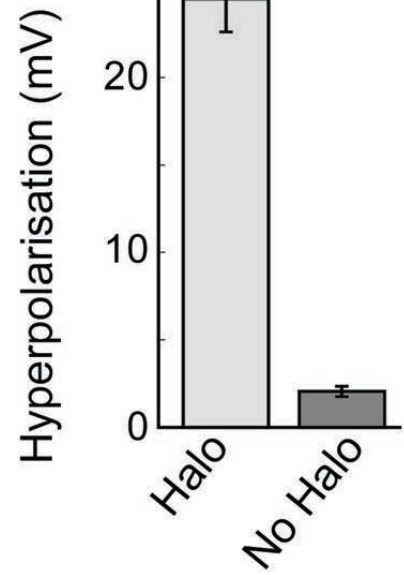




Ai. Direct / indirect effects on Em



Bi.



Bii.

